International Journal of Heat and Mass Transfer 54 (2011) 1064–1070

Contents lists available at ScienceDirect

International Journal of Heat and Mass Transfer

journal homepage: www.elsevier.com/locate/ijhmt

# Enhancement of specific heat capacity of high-temperature silica-nanofluids synthesized in alkali chloride salt eutectics for solar thermal-energy storage applications

Donghyun Shin, Debjyoti Banerjee *

*Department of Mechanical Engineering, Texas A&M University, College Station, TX 77843 3123, United States*

ARTICLE INFO

*Article history:*
Received 19 June 2010
Accepted 2 November 2010
Available online 13 December 2010

*Keywords:*
Nanoparticle
Specific heat capacity
Alkali chloride eutectic
Silicon dioxide
Electron microscopy

ABSTRACT

In this study, we report the anomalous enhancement of specific heat capacity of high-temperature nanofluids. Alkali metal chloride salt eutectics were doped with silica nanoparticles at 1% mass concentration. The specific heat capacity of the nanofluid was enhanced by 14.5%. Dispersion behavior of the nanoparticles in the eutectic was confirmed by scanning electron microscopy (SEM). Three independent competing transport mechanisms are enumerated to explain this anomalous behavior.

© 2010 Elsevier Ltd. All rights reserved.

## 1. Introduction

Solvents doped with stable suspensions of nanoparticles at minute concentrations are termed as "nanofluids" [1–3]. Nanoparticles are defined as distinct solid particles with a nominal size in the range of 1–100 nm [4]. Nanofluids were reported for the anomalous enhancement of thermal conductivity over that of the neat solvent. Eastman et al. [5] reported thermal conductivity enhancement of 30% and 60% for water based nanofluids of $Al_2O_3$ and CuO, respectively, at 5% volume concentration. Xuan and Li [6] reported thermal conductivity enhancement of 54% for water based nanofluids using copper nanoparticles at 5% volume concentration. Murshed et al. [7] observed 30% enhancement of thermal conductivity of water based $TiO_2$ nanofluid at 5% volume concentration. Choi et al. [8] observed 160% enhancement of thermal conductivity for multi-walled carbon nanotube dispersed into oil at 1% concentration by volume. Eastman et al. [5] observed 44% enhancement in thermal conductivity at only 0.052% volume concentration of copper nanoparticles in oil. Kang et al. [9] reported that for ethylene glycol based diamond nanofluid the thermal conductivity was enhanced by 75% at 1.32% volume concentration of diamond nanoparticles. Das et al. [10] explored $Al_2O_3$ and CuO nanofluids and observed temperature dependency of thermal conductivity enhancement. Patel et al. [11] observed thermal conductivity of Ag nanofluid enhanced by 21% for only 0.00026% volume concentration. Several studies have been performed to explain the anomalous enhancement of thermal conductivity of nanofluids [12–17]. Recent studies proposed that percolation network within cluster of nanoparticles due to aggregation may be primarily responsible for the enhancement of the nanofluids [18,19].

Similarly, specific heat capacity of solvents can also be enhanced by doping with nanoparticles. Nelson et al. [20] reported that the specific heat capacity of polyalphaolefin was enhanced by 50% on addition of ex-foliated graphite nanoparticles at 0.6% concentration by weight. Shin and Banerjee [21] synthesized molten salt-based silica nanofluid and observed 26% enhanced specific heat capacity for 1% weight concentration. On the contrary, Zhou and Ni [22] reported that the specific heat capacity of water based $Al_2O_3$ nanofluid decreased by 40–50% at 21.7% volume concentration of $Al_2O_3$. However, $Al_2O_3$ nanoparticles are likely to agglomerate and precipitate since $Al_2O_3$ is not soluble in water. It is necessary to control the pH of the nanofluids within close tolerances for the $Al_2O_3$ nanoparticles to remain in suspension and to be well dispersed in water. However, in this study the authors did not verify (or report) whether the nanoparticles were well dispersed and if they were not agglomerated. It is possible that the nanoparticles were agglomerated and precipitated out of the water based solution, resulting in degradation of the thermal properties.

Solar energy conversion to electricity is achieved primarily by using (a) photovoltaic technology, or (b) by harnessing solar thermal-energy. At larger scales of production, solar thermal

* Corresponding author. Tel.: +1 979 845 4500; fax: +1 979 845 3081.
*E-mail address:* dbanerjee@tamu.edu (D. Banerjee).

0017-9310/$ - see front matter © 2010 Elsevier Ltd. All rights reserved.
doi:10.1016/j.ijheatmasstransfer.2010.11.017

**Nomenclature**

| | |
|---|---|
| $C_p$ | specific heat capacity |
| *Greek symbols* | |
| $\rho$ | density |
| $\phi$ | volume fraction |
| *Subscripts* | |
| $f$ | fluid properties |
| $p$ | solid (nanoparticle) properties |
| $t$ | total/cumulative (nanofluid) properties |

techniques are more reliable and cost effective (as opposed to photovoltaic technologies), since these platforms can provide uninterrupted power supply in the off peak time (at night and during cloud cover). Solar thermal power plants rely on high temperature thermal storage units for continuous operation. Typical solar thermal-energy storage facilities require the storage medium to have high heat capacity and thermal conductivity. Contemporary commercial solar thermal units use energy storage facilities that operate at ~400 °C and typically use mineral oil based storage medium as well as heat transfer fluids. It is estimated that pushing the storage facility to operate at ~500–600 °C or higher can make the cost of solar power competitive with coal fired power plants in near future [23]. However, few materials are compatible with the cost and performance requirements for such high-temperature thermal-energy storage. Typical materials used as HTF and for high-temperature thermal-energy storage include Na–K eutectics and alkali metal salt eutectics (e.g., $NaNO_3$, $KNO_3$, KCl, etc.). However, these materials have low thermo-physical properties. Hence, there is a need to find better performing thermal-energy storage technologies and materials that are cost effective. It should be noted that novel materials (such as nano-material additives) can become cost-effective if they can increase the operating range of the storage facilities to higher range of temperatures. For high-temperature thermal-energy storage, compatible materials include molten salts and their eutectics, such as alkali-nitrate, alkali-carbonate, or alkali-chlorides. However, those molten salts have relatively low heat capacity – usually less than 0.8 J/g K (in contrast to specific heat capacity of water which is 4.1 J/g K at room temperature).

The objective of this study is to measure the change in specific heat capacity of molten salt eutectics by doping them with minute amount of nanoparticles, thus realizing high temperature nanofluids for the thermal energy storage applications. In this study, silicon dioxide nanoparticles at 1% concentration by weight were dispersed in a eutectic of alkali chloride salts ($BaCl_2$, NaCl, $CaCl_2$, and LiCl). The pure eutectic has a melting point of 378 °C [24]. Then, the specific heat capacities of the eutectic as well as the silica nanofluid were measured using a differential scanning calorimeter (Model: Q20, TA Instruments, Inc.). The specific heat capacity of the $SiO_2$ nanofluid is then compared with the theoretical predictions from the thermal equilibrium model for mixtures of materials [25]:

$$c_{p,t} = \frac{\phi_p \rho_p c_{p,p} + \phi_f \rho_f c_{p,f}}{\phi_p \rho_p + \phi_f \rho_f} \quad (1)$$

where $c_{p,t}$ is effective specific heat capacity of mixture, $c_{p,f}$ is specific heat capacity of fluid, $c_{p,p}$ is specific heat capacity of particle, $\phi_p$ is volume fraction of particle, $\phi_f$ is volume fraction of fluid, $\rho_p$ is density of particle, and $\rho_f$ is density of fluid.

Nanofluid properties are degraded if the nanoparticles do not dissolve properly in the base liquid. Dissolution of nanoparticles ensures more homogeneous composition and helps to enhance the thermo-physical properties of the nanofluids. Dissolution of nanoparticles is accompanied by more uniform dispersion of the nanoparticles and this helps to prevent or minimize the agglomeration of the nanoparticles [4]. In this study, uniform dispersion and minimal amount of agglomeration is observed and confirmed by scanning electron microscopy.

## 2. Experimental procedure

The general protocol for preparing the nanofluid is as follows (Fig. 1): 68.490 mg of barium chloride, 24.784 mg of sodium chloride, 79.206 mg of calcium chloride, 25.520 mg of lithium chloride, and 2 mg of silicon dioxide were measured in advance on a balance. The pure eutectic was prepared in the same manner without adding the silicon dioxide nanoparticles. All chemicals were then dissolved in 20 ml of distilled water. This water solution, which contains 1% of $SiO_2$/chloride eutectic nanofluid, was sonicated by an ultra sonicater (Branson 3510, Branson Ultrasonics Corporation) for ~100 min. to obtain homogeneous dispersion of the nanofluid. The water solution was then rapidly evaporated on a hot plate (C-MAG HP7, IKA), which was maintained at 200 °C. A portion of the dry sample was transferred to a Tzero hermetic pan (for subsequent DSC measurements). The pan was then mounted on a hotplate to remove any absorbed moisture. The standard Tzero hermetic pan was fixed with a lid (TA Instruments, Inc.) and hermetically sealed. Before transferring the samples to the pan, the empty pan/lid and the pan/lid with a sapphire reference (25.412 mg) were mounted in a differential scanning calorimeter (Q20, TA Instruments, Inc.) to obtain a baseline and a reference data. A custom temperature program which follows the standard DSC test method (ASTM-E1269) was created for these measurements. The temperature was initially held at 150 °C for at least 4 min. to evaporate any adsorbed moisture. The temperature was then ramped up to 560 °C at 20 °C/min. and held for another 4 min. The DSC was then cooled down to room temperature. The same temperature program was then cycled 4–6 times with the same sample to test repeatability of the sample.

The size of the nanoparticles in the nanofluid samples were also measured before and after performing the DSC experiments using a scanning electron microscope (JEOL JSM-7500F).

## 3. Measurement uncertainty

The precision of the heat flow measurements in the DSC instrument is 1 mJ ($10^{-3}$ J). It is shown in Table 1 that the standard deviation in the measurement for the different nanofluid samples varies from 0.02 J/g K to 0.04 J/g K. Hence, the measurement uncertainty in the experiments is estimated to be in the range 2–4%. This shows that the heat capacity enhancements observed in this study are significantly higher than the measurement uncertainties.

## 4. Data analyses

The results from the DSC measurement are shown in Fig. 2 and Table 1. The specific heat capacity of both chloride eutectic and nanofluid seems to be constant at liquid phase. This result is consistent with literature data for the pure (neat) chloride eutectic. According to Janz et al. [24], the specific heat capacity of eutectic of molten salt is constant for the liquid phase. Araki et al. [26]

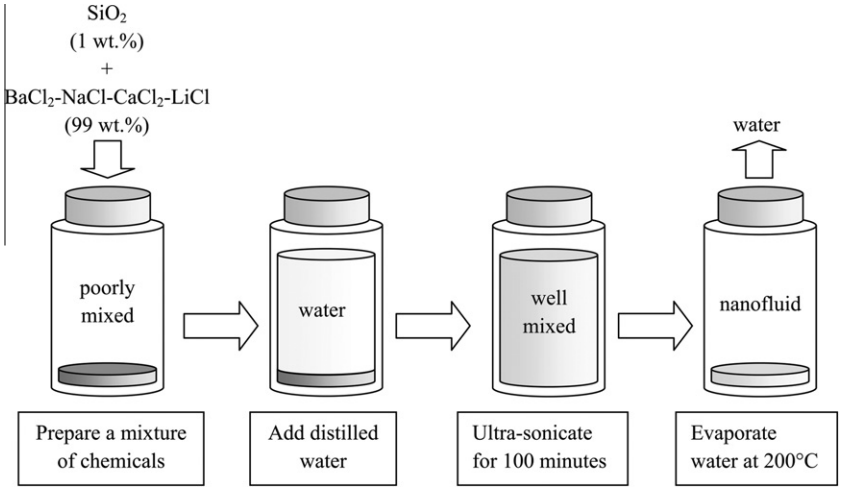


**Fig. 1.** The general protocol for preparing the nanofluid (liquid solution method).

**Table 1**
Specific heat capacity measurements for pure eutectic of chloride salts and the eutectic doped with $SiO_2$ nanoparticles at 1% mass concentration.

| | Base chloride Sample #1 | Base chloride Sample #2 | $SiO_2$ nanofluid Sample #1 | $SiO_2$ nanofluid Sample #2 |
|---|---|---|---|---|
| 1st run | 0.82 J/g °C | 0.82 J/g°C | 0.93 J/g °C | 0.92 J/g °C |
| 2nd run | 0.80 J/g °C | 0.85 J/g°C | 0.96 J/g °C | 0.95 J/g °C |
| 3rd run | 0.82 J/g °C | 0.86 J/g°C | 0.96 J/g °C | 0.97 J/g °C |
| 4th run | 0.84 J/g °C | 0.88 J/g°C | 0.97 J/g °C | 1.01 J/g °C |
| 5th run | 0.87 J/g °C | | | 1.03 J/g °C |
| 6th run | 0.89 J/g °C | | | 1.01 J/g °C |
| Average | 0.84 J/g °C | 0.86 J/g °C | 0.96 J/g °C | 0.99 J/g °C |
| Standard deviation | 0.03 | 0.02 | 0.02 | 0.04 |

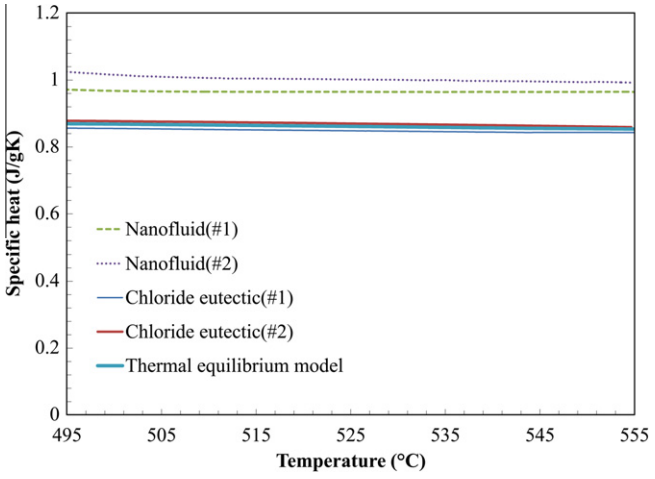


**Fig. 2.** Variation of the specific heat capacity of pure eutectic and nanofluid with temperature. Theoretical model based on thermal equilibrium is shown in the figure for comparison. The theoretical estimate for the nanofluid is not different from the pure eutectic. However, experimental measurements at 1% weight concentration of $SiO_2$ nanofluid shows enhancements of ~14.5% in the liquid phase. This anomalous enhancement demonstrates alternate transport mechanisms in nanofluids that are not accounted for in the theoretical model (“Thermal Equilibrium Model”, Eq. (1), [25]).

measured specific heat capacity of molten salt and reported that it remains constant for the liquid phase, while the specific heat capacity of solid phase was reported to increase with temperature. The average specific heat capacity of chloride eutectics (#1 and #2) between 500 °C and 555 °C were measured to be 0.85 J/g K and 0.87 J/g K, respectively. The average specific heat capacity of $SiO_2$ nanofluids (#1 and #2) was measured to be 0.97 J/g K and 1.00 J/g K, respectively. The average enhancement on the specific heat capacity was thus observed to be 14.5%. However, the existing theoretical models (e.g., Eq. (1), [25]) cannot explain this anomalous enhancement of the specific heat capacity at such low concentrations of the nanoparticles (~0.6% by volume). This result implies that alternate transport mechanisms exist for nanofluids, thus distinguishing nanofluids from a simple mixture of two materials.

## 5. Results

Since nanoparticles have a propensity to agglomerate and precipitate if the liquid properties (such as pH) are not controlled within close tolerances, it is necessary to examine whether or not nanoparticles are well dispersed and unagglomerated before and after thermal cycling. The high-temperature nanofluid samples were subjected to rapid melting/solidification and temperature cycles, and therefore it is necessary to ensure that the nanoparticles are not agglomerated and are well dispersed after the measurements are performed. Fig. 3 is an SEM image of $SiO_2$ nanofluid before melting/solidification in the DSC, while Fig. 4 is an SEM image of $SiO_2$ nanofluid after melting and solidification several times in the DSC. Fig. 4 shows that the rapid thermal cycling did not cause any significant agglomeration of the nanoparticles in the eutectic. The average diameter of $SiO_2$ nanoparticles in the Fig. 3 is ~26 nm (before temperature cycling). The average diameter of the silica nanoparticles observed in Fig. 4 is ~27 nm. It is shown in Fig. 3 and 4 that $SiO_2$ nanoparticles are uniformly dispersed before running in the DSC and the dispersion did not change after melting/solidification. Close

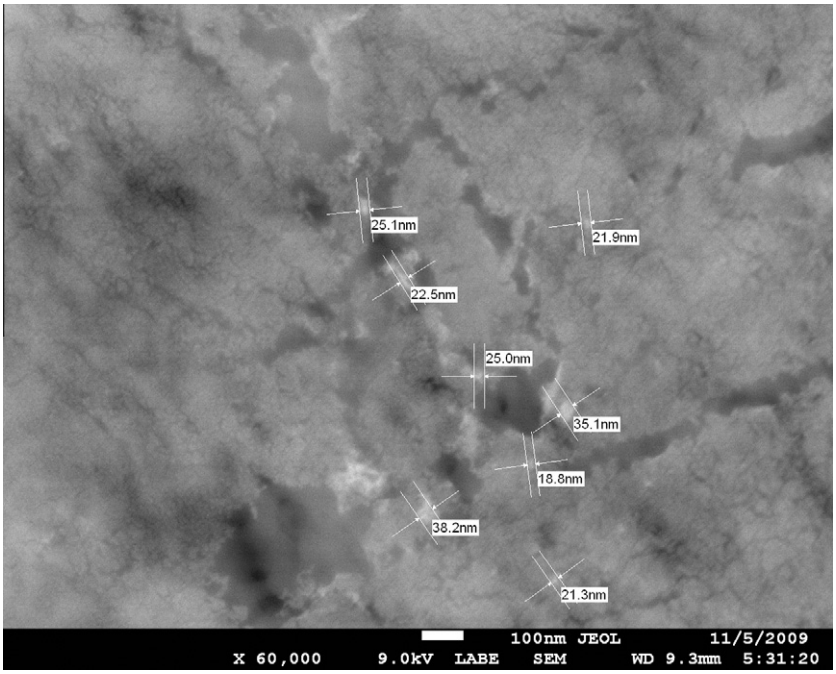


**Fig. 3.** SEM image of $SiO_2$ nanofluid before melting in the DSC. The average diameter of $SiO_2$ nanoparticles is ~26 nm. The nanoparticles are uniformly dispersed and no agglomeration is observed.

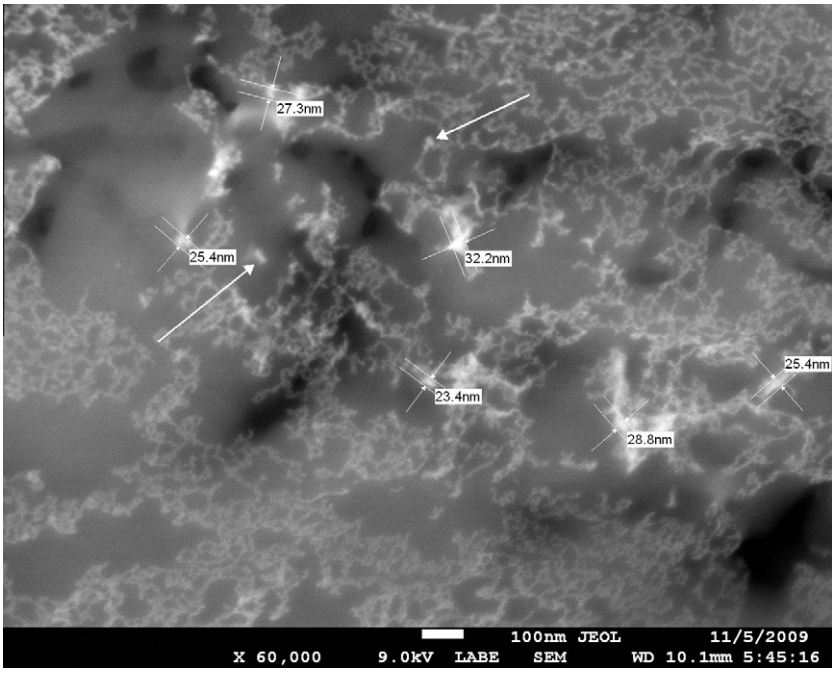


**Fig. 4.** SEM image of $SiO_2$ nanofluid after repeated thermal cycling involving melting and solidification in the DSC. The average diameter of $SiO_2$ nanoparticles is ~27 nm. The nanoparticles are uniformly dispersed and no agglomeration is observed after thermal cycling and melting/solidification cycles in the DSC. A special substructure of higher density layer is observed in the eutectic surrounding the nanoparticles, forming a percolation type network.

examination of Fig. 4 shows that a network substructure forms in the eutectic in the location of the nanoparticles. The alkali salt material appears to be of a higher density in the vicinity of the nanoparticles and appears to be of a lighter color. The substructure seems to interconnect the $SiO_2$ nanoparticles, thus forming a percolation network. For comparison, a SEM image of the pure eutectic after multiple thermal cycling is presented in Fig. 5. The interconnected network was not observed in the pure eutectic. This network could be formed due to the adhesion layer of the eutectic molecules around the nanoparticles that potentially have semi-solid properties, such as higher density, specific heat capacity and thermal conductivity (as well as higher viscosity in the semi-solid/liquid state). This interconnected network formed due to the presence of the nanoparticles in the eutectic may be one of the factors that are responsible for enhancing thermal properties of the nanofluid. The other modes or mechanisms responsible for the anomalous enhancement of specific heat capacity of the nanofluid are discussed next.

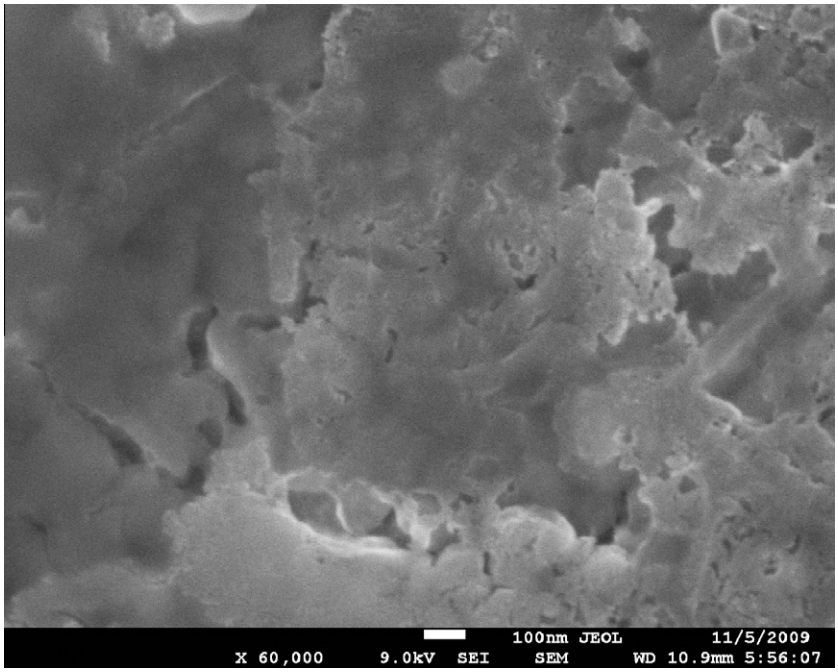


**Fig. 5.** SEM image of pure eutectic after repeated thermal cycling involving melting and solidification in the DSC. A special substructure, which was shown in the nanofluid (Fig. 3), was not observed in the pure eutectic.

## 6. Discussion

The anomalous enhancement of the specific heat capacity can be explained by three independent competing inter-molecular interaction mechanisms (or modes). These three modes are discussed next.

*Mode I. Higher specific heat capacity of nanoparticles than the bulk value of silica:* (Fig. 6) Literature reports show that the specific heat capacity of particles can be enhanced up to 25% (compared to bulk property values) due to the high surface energy per unit mass of the nanoparticle. Wang et al. [27] used a theoretical model and reported that the specific heat capacity of nanoparticle was enhanced when the size of the nanoparticle is decreased. Experimentally, specific heat capacity of $Al_2O_3$ nanoparticle was observed to increase by up to 25% compared with the bulk value property value of $Al_2O_3$ [28]. Hence, for nanometer-sized particles, the specific heat in Eq. (1) should be a function of the nominal nanoparticle diameter. The surface atoms in the lattice of the nanoparticle are less constrained due to the less number of bonds. Since the bonds can be "visualized" to act like springs – the surface atoms vibrate at a lower natural frequency and higher amplitudes – resulting in higher surface energy. Hence, the phonon spectrums of nanoparticles are quantized and have discrete values which are constrained by the size of the nanoparticle.

*Mode* II. Solid–Fluid interaction energy: (Fig. 7) Furthermore, extremely high surface area per unit mass of nanoparticles cause an anomalous increase in the interfacial thermal resistance between the nanoparticles and surrounding liquid molecules, which is usually negligible in macro scale. This high interfacial thermal resistance should act as additional thermal storage due to the interfacial interaction of the vibration energies between nanoparticle atoms and the interfacial molecules [16,29].

*Mode III. "Layering" of liquid molecules at surface to form semi-solid layer:* (Fig. 8) In addition, liquid molecules adhering on the surface of the nanoparticles have a semi-solid behavior. The thickness of this "adhesion layer" of liquid molecules would depend on the surface energy of the nanoparticle. These semi-solid layers usually have higher thermal properties than the bulk liquid and therefore contribute to increasing the effective specific heat capacity of nanofluid. Li et al. [30] performed an equilibrium

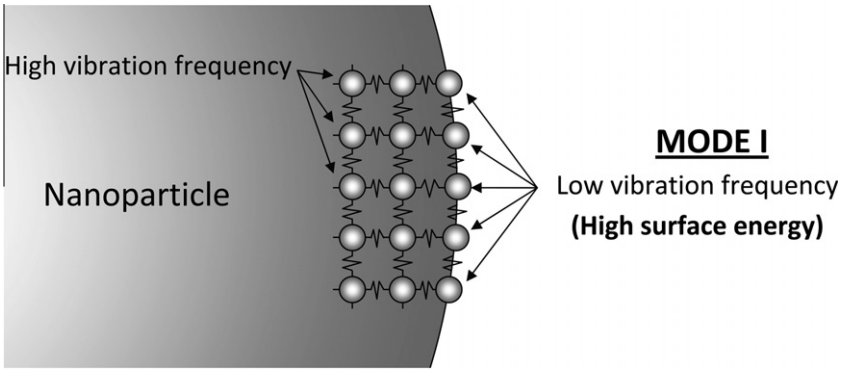


**Fig. 6.** Schematic showing Mode I of energy storage arising from high surface energy of the surface atoms in the lattice (low vibration frequency and higher amplitudes of vibration leading to higher surface energy).

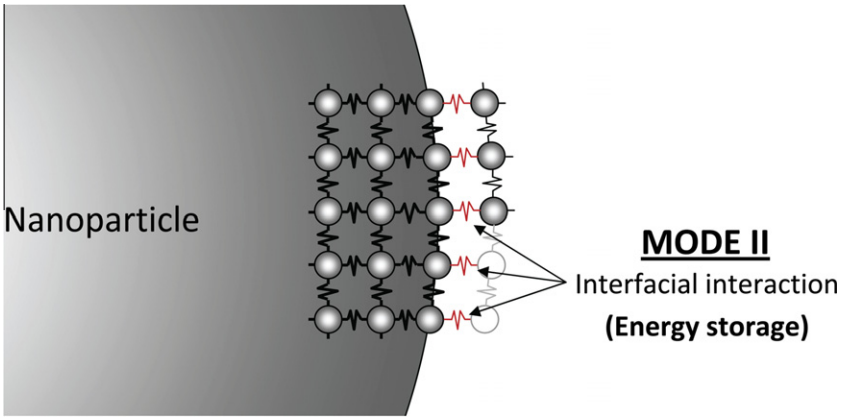


**Fig. 7.** Schematic showing Mode II of energy storage arising from interfacial interactions between liquid molecules and lattice atoms – which act as virtual spring-mass systems.

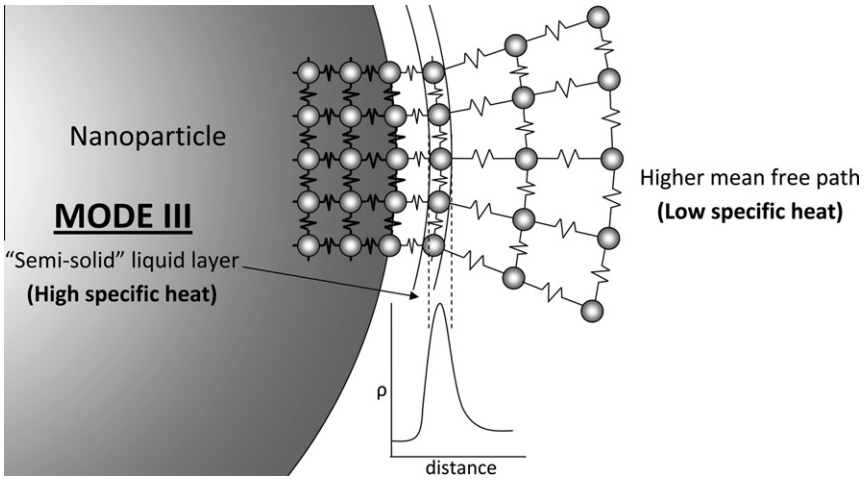


**Fig. 8.** Schematic showing Mode III of energy storage arising from a layer of semi-solid molecules adhering to the surface lattice-atoms. The layer of semi-sold molecules is expected to have a higher specific heat capacity due to the reduced inter-molecular spacing and semi-solid behavior of this layer. Such a layer of semi-solid molecules would not exist in the absence of the nano-particles (key: $\rho$ = mass density; units: kg/m$^3$).

molecular dynamics simulation to demonstrate the existence of the semi-solid layer surrounding a nanoparticle. Oh et al. [31] reported TEM images to show the experimental evidence for ordering of liquid molecules on the interface between liquid aluminum and sapphire. Ample evidence exists in the molecular dynamics literature that shows that this semi-solid layer of liquid molecules on a crystalline surface is constrained to a region that is ~2–5 nm in thickness, which is about ~10 molecules or less in thickness. The numbers of adhered layers of the liquid molecules are expected to be a function of the surface energy of the crystalline interface. The mass fraction of the adhered ''semi-solid'' molecules is expected to increase proportionally on a nanoparticle surface with the reduction in the size (for the same concentration of nanoparticles by weight).

Thus, for a given concentration (mass fraction) of the nanoparticles – an optimum diameter of the nanoparticle can also be expected to exist in order to maximize the mass fraction of the adhered molecules from the liquid-phase forming the semi-solid layer – and thus providing an optimum in the enhancement of the specific heat capacity of the nanofluid. In addition, the optimum concentration of the nanoparticles can be a function of the nanoparticle nominal size or the size distribution of the nanoparticles (this is the subject of future studies by our research group).

## 7. Conclusion

In conclusion, specific heat capacity of neat chloride eutectics and their nanofluids obtained by doping with $SiO_2$ nanoparticles (at 1% weight concentration) with ~20–30 nm nominal diameter – were explored in this study. The $SiO_2$ nanofluid enhanced the specific heat capacity by 14.5% compared with that of the neat chloride salt eutectic. This enhancement is significantly higher than the measurement uncertainty of 2–4%. This anomalous enhancement of the specific heat capacity confirms a previous report by the authors on this topic and also contradicts a previous study reported in the literature (which was probably due to agglomeration/precipitation of the nanoparticles from the solution). Three independent thermal transport mechanisms were proposed to explain the unusual enhancement of the specific heat capacity: (1) Mode I: enhanced specific heat capacity of nanoparticle due to higher specific surface energy (compared with bulk material); (2) Mode II: additional thermal storage mechanisms due to interfacial interactions (e.g., such as interfacial thermal resistance and capacitance) between nanoparticle and the adhering liquid molecules due to the extremely high specific surface area of the nanoparticle; and (3) Mode III: the existence of semi-solid liquid layer adhering to the nanoparticles, which are likely to have

enhanced specific heat capacity due to the smaller inter-molecular spacing similar to the nanoparticle lattice structure on the surface (compared to the higher inter-molecular spacing in the bulk liquid). The authors hope that this finding of anomalous enhancement of specific heat capacity of nanofluids will raise the interest level of the scientific community for further research into this topic, which currently receives less attention than research on, say, anomalous enhancement of thermal conductivity of nanofluids.

## Acknowledgements

The authors acknowledge the support of the Department of Energy (DOE) Solar Energy Program (Golden, CO) under Grant No. DE-FG36-08GO18154; Amd. M001 (Title: ''Molten Salt-Carbon Nanotube Thermal Energy Storage For Concentrating Solar Power Systems'').

## References

[1] D. Wen, G. Lin, S. Vafaei, K. Zhang, Review of nanofluids for heat transfer applications, Particuology 7 (2009) 141–150.
[2] X.-Q. Wang, A.S. Majumdar, Heat transfer characteristics of nanofluids: a review, Int. J. Therm. Sci. 46 (2007) 1–19.
[3] P. Keblinski, J.A. Eastman, D.G. Cahill, Nanofluids for thermal transport, Mater. Today 8 (2005) 36–44.
[4] K. Henderson, Y.-G. Park, L. Liu, A.M. Jacobi, Flow-boiling heat transfer of R-134a-based nanofluids in a horizontal tube, Int. J. Heat Mass Transfer 53 (2009) 944–951.
[5] J.A. Eastman, S.U.S. Choi, S. Li, L.J. Thompson, Enhanced thermal conductivity through the development of nanofluids, in: Proceedings of the Symposium on Nanophase and Nanocomposite Materials II, vol. 457, Materials Research Society, 1997, pp. 3–11.
[6] Y. Xuan, Q. Li, Heat transfer enhancement of nanofluids, Int. J. Heat Fluid Flow 21 (2000) 58–64.
[7] S.M.S. Murshed, K.C. Leong, C. Yang, Enhanced thermal conductivity of $TiO_2$–water based nanofluids, Int. J. Therm. Sci. 44 (2005) 367–373.
[8] S.U.S. Choi, Z.G. Zhang, F.E. Lockwood, E.A. Grulke, Anomalous thermal conductivity enhancement in nanotubes suspensions, Appl. Phys. Lett. 79 (2001) 2252–2254.
[9] H.U. Kang, S.H. Kim, J.M. Oh, Estimation of thermal conductivity of nanofluid using experimental effective particle volume, Exp. Heat Transfer 19 (2006) 181–191.
[10] S.K. Das, N. Putra, P. Thiesen, W. Roetzel, Temperature dependence of thermal conductivity enhancement for nanofluids, ASME J. Heat Transfer 125 (2003) 567–574.
[11] H.E. Patel, S.K. Das, T. Sundararagan, A.S. Nair, B. Geoge, T. Pradeep, Thermal conductivities of naked and monolayer protected metal nanoparticle based nanofluids: manifestation of anomalous enhancement and chemical effects, Appl. Phys. Lett. 83 (2003) 2931–2933.
[12] Y. Xuan, W. Roetzel, Conceptions for heat transfer correlation of nanofluids, Int. J. Heat Mass Transfer 43 (2000) 3701–3707.
[13] P. Keblinski, S.R. Phillpot, S.U.S. Choi, J.A. Eastman, Mechanisms of heat flow in suspensions of nano-sized particles (nanofluids), Int. J. Heat Mass Transfer 45 (2002) 855–863.
[14] D.H. Kumar, H.E. Patel, V.R.R. Kumar, T. Sundararajan, T. Pradeep, S.K. Das, Model for heat conduction in nanofluids, Phys. Rev. Lett. 93 (2004) 144301.
[15] S.P. Jang, S.U.S. Choi, Role of Brownian motion in the enhanced thermal conductivity of nanofluids, Appl. Phys. Lett. 84 (2004) 4316–4318.
[16] R. Prasher, P. Bhattacharya, P.E. Phelan, Brownian-motion-based convective–conductive model for the effective thermal conductivity of nanofluids, ASME J. Heat Transfer 128 (2006) 588–595.
[17] H.E. Patel, T. Sundararajan, S.K. Das, A cell model approach for thermal conductivity of nanofluids, J. Nanoparticle Res. 10 (2008) 87–97.
[18] P. Keblinski, R. Prasher, J. Eapen, Thermal conductance of nanofluids: is the controversy over?, J Nanoparticle Res. 10 (2008) 1089–1097.
[19] W. Evans, R. Prasher, J. Fish, P. Meakin, P. Phelan, P. Keblinski, Effect of aggregation and interfacial thermal resistance on thermal conductivity of nanocomposite and colloidal nanofluids, Int. J. Heat Mass Transfer 51 (2008) 1431–1438.
[20] I.C. Nelson, D. Banerjee, R. Ponnappan, Flow loop experiments using polyalphaolefin, J. Thermophys. Heat Transfer 23 (2009) 752–761.
[21] D. Shin, D. Banerjee, Enhanced specific heat of silica nanofluid, ASME J. Heat Transfer 133 (2011) 024501–024504, doi:10.1115/1.4002600.
[22] S.Q. Zhou, R. Ni, Measurement of the specific heat capacity of water-based $Al_2O_3$ nanofluid, Appl. Phys. Lett. 92 (2008) 093123.
[23] H. Price, E. Lüpfert, D. Kearney, E. Zarza, G. Cohen, R. Gee, R. Mahoney, Advances in parabolic trough solar power technology, J. Solar Energy Eng. 124 (2002) 109–125.
[24] G.J. Janz, C.B. Allen, N.P. Bansal, R.M. Murphy, R.P.T. Tomkins, Physical Properties Data Compilations Relevant to Energy Storage, II. Molten Salts: Data on Single and Multi-component Systems, US Govt. Print. Off., Washington, DC, 1979, p. 431.
[25] J. Buongiorno, Convective transport in nanofluids, J. Heat Transfer 128 (2006) 240–250.
[26] N. Araki, M. Matsuura, A. Makino, T. Hirata, Y. Kato, Measurement of thermophysical properties of molten salts: Mixtures of alkaline carbonate salts, Int. J. Thermophys. 9 (2005) 1071–1080.
[27] B.X. Wang, L.P. Zhou, X.F. Peng, Surface and size effects on the specific heat capacity of nanoparticles, Int. J. Thermophys. 27 (2006) 139–151.
[28] L. Wang, Z. Tan, S. Meng, D. Liang, G. Li, Enhancement of molar heat capacity of nanostructured $Al_2O_3$, J. Nanoparticle Res. 3 (2004) 483–487.
[29] L. Xue, P. Keblinski, S.R. Phillpot, S.U.-S. Choi, J.A. Eastman, Effect of liquid layering at the liquid–solid interface on thermal transport, Int. J. Heat Mass Transfer 47 (2004) 4277–4284.
[30] L. Li, Y. Zhang, H. Ma, M. Yang, Molecular dynamics simulation of effect of liquid layering around the nanoparticle on the enhanced thermal conductivity of nanofluids, J. Nanoparticle Res. 12 (2010) 811–821.
[31] S.H. Oh, Y. Kauffmann, C. Scheu, W.D. Kaplan, M. Rühle, Ordered liquid aluminum at the interface with sapphire, Science 310 (2005) 661–663.